

# Reactor Fuel Fraction Information on the Antineutrino Anomaly

C. Giunti

*INFN, Sezione di Torino, Via P. Giuria 1, I-10125 Torino, Italy*

X.P. Ji

*Department of Engineering Physics, Tsinghua University, Beijing 100084, China*

M. Laveder

*Dipartimento di Fisica e Astronomia “G. Galilei”, Università di Padova,  
and INFN, Sezione di Padova, Via F. Marzolo 8, I-35131 Padova, Italy*

Y.F. Li

*Institute of High Energy Physics, Chinese Academy of Sciences, and School of Physical Sciences,  
University of Chinese Academy of Sciences, Beijing 100049, China*

B.R. Littlejohn

*Illinois Institute of Technology, Chicago, IL 60616, USA*

(Dated: 3 August 2017)

We analyzed the evolution data of the Daya Bay reactor neutrino experiment in terms of short-baseline active-sterile neutrino oscillations taking into account the theoretical uncertainties of the reactor antineutrino fluxes. We found that oscillations are disfavored at  $2.6\sigma$  with respect to a suppression of the  $^{235}\text{U}$  reactor antineutrino flux and at  $2.5\sigma$  with respect to variations of the  $^{235}\text{U}$  and  $^{239}\text{Pu}$  fluxes. On the other hand, the analysis of the rates of the short-baseline reactor neutrino experiments favor active-sterile neutrino oscillations and disfavor the suppression of the  $^{235}\text{U}$  flux at  $3.1\sigma$  and variations of the  $^{235}\text{U}$  and  $^{239}\text{Pu}$  fluxes at  $2.8\sigma$ . We also found that both the Daya Bay evolution data and the global rate data are well-fitted with composite hypotheses including variations of the  $^{235}\text{U}$  or  $^{239}\text{Pu}$  fluxes in addition to active-sterile neutrino oscillations. A combined analysis of the Daya Bay evolution data and the global rate data shows a slight preference for oscillations with respect to variations of the  $^{235}\text{U}$  and  $^{239}\text{Pu}$  fluxes. However, the best fits of the combined data are given by the composite models, with a preference for the model with an enhancement of the  $^{239}\text{Pu}$  flux and relatively large oscillations.

PACS numbers: 28.41.-i, 14.60.Pq, 14.60.St

## I. INTRODUCTION

The Daya Bay collaboration presented recently [1] the results of the measurement of the correlation between the reactor fuel evolution and the changes in the antineutrino detection rate which is quantified by the cross section per fission  $\sigma_f$ , given by

$$\sigma_f = \sum_i F_i^a \sigma_{f,i}, \quad (1)$$

where  $F_i^a$  and  $\sigma_{f,i}$  are the effective fission fractions and the cross sections per fission of the four fissionable isotopes  $^{235}\text{U}$ ,  $^{238}\text{U}$ ,  $^{239}\text{Pu}$ ,  $^{241}\text{Pu}$ , denoted, respectively, with the label  $i = 235, 238, 239, 241$ .

The Daya Bay collaboration presented in Fig. 2 of Ref. [1] the values of  $\sigma_f$  for eight values of the effective  $^{239}\text{Pu}$  fission fraction  $F_{239}$ . They fitted these data allowing variations of the two main cross sections per fission  $\sigma_{f,235}$  and  $\sigma_{f,239}$ , with the assumption that  $\sigma_{f,238}$  and  $\sigma_{f,241}$  have the Saclay+Huber theoretical values [2–4] with enlarged 10% uncertainties. They also compared the best-fit of this analysis with the best-fit obtained under the hypothesis of active-sterile neutrino oscillations,

which predicts the same suppression for the four cross sections per fission with respect to their theoretical value. They obtained  $\Delta\chi^2/\text{NDF} = 7.9/1$ , corresponding to a  $p$ -value of 0.49%, which disfavors the active-sterile oscillations hypothesis by  $2.8\sigma$ . In this calculation the uncertainties of the theoretical calculation of the four cross sections per fission were not taken into account.

In this paper we present the results of analyses of the Daya Bay evolution data [1] with least-squares functions that take into account explicitly the uncertainties of the theoretical calculation of the four cross sections per fission. Moreover, we consider additional models with independent variations of the  $^{235}\text{U}$  and  $^{239}\text{Pu}$  fluxes with and without active-sterile neutrino oscillations, and we extend the analysis taking into account also the information on the cross sections per fission of all the other reactor antineutrino experiments which have different fuel fractions. We also perform proper statistical comparisons of the non-nested models under consideration through Monte Carlo estimations of the  $p$ -values.

Given a set of data labeled with the index  $a$  on the cross section per fission for different values of the fuel

fractions, we write the theoretical predictions as

$$\sigma_{f,a}^{\text{th}} = \sum_i F_i^a r_i \sigma_{f,i}^{\text{SH}}, \quad (2)$$

where  $i = 235, 238, 239, 241$  and  $\sigma_{f,i}^{\text{SH}}$  are the Saclay+Huber cross sections per fission. The coefficients  $r_i$  are introduced in order to take into account the uncertainties of the Saclay+Huber cross sections per fission or to study independent variations of the antineutrino fluxes from the four fissionable isotopes with respect to the Saclay+Huber theoretical values [2–4].

We consider the following models:

**235:** A variation of the cross section per fission of the antineutrino flux from  $^{235}\text{U}$  only.

In this case, we analyze the data with the least-squares statistic

$$\chi^2 = \sum_{a,b} \left( \sigma_{f,a}^{\text{th}} - \sigma_{f,a}^{\text{exp}} \right) (V_{\text{exp}}^{-1})_{ab} \left( \sigma_{f,b}^{\text{th}} - \sigma_{f,b}^{\text{exp}} \right) + \sum_{i,j=238,239,241} (r_i - 1) (V_{\text{SH}}^{-1})_{ij} (r_j - 1), \quad (3)$$

where  $\sigma_{f,a}^{\text{exp}}$  are the measured cross sections per fission,  $V_{\text{exp}}$  is the experimental covariance matrix, and  $V_{\text{SH}}$  is the covariance matrix of the fractional uncertainties of the Saclay-Huber theoretical calculation of the antineutrino fluxes from the four fissionable isotopes (given in Table 3 of Ref. [5]).

In this analysis there is only one parameter determined by the fit:  $r_{235}$ . The parameters  $r_{238}$ ,  $r_{239}$ , and  $r_{241}$  are nuisance parameters.

**235+239:** Independent variations of the cross sections per fission of the antineutrino fluxes from  $^{235}\text{U}$  and  $^{239}\text{Pu}$ .

In this case, we analyze the data with the least-squares statistic

$$\chi^2 = \sum_{a,b} \left( \sigma_{f,a}^{\text{th}} - \sigma_{f,a}^{\text{exp}} \right) (V_{\text{exp}}^{-1})_{ab} \left( \sigma_{f,b}^{\text{th}} - \sigma_{f,b}^{\text{exp}} \right) + \sum_{i,j=238,241} (r_i - 1) (V_{\text{SH}}^{-1})_{ij} (r_j - 1). \quad (4)$$

In this analysis there are two parameters determined by the fit:  $r_{235}$  and  $r_{239}$ . The parameters  $r_{238}$  and  $r_{241}$  are nuisance parameters.

**OSC:** Active-sterile neutrino oscillations, in which the measured cross sections per fission are suppressed with respect to the theoretical cross sections per fission  $\sigma_{f,a}^{\text{th}}$  by the survival probability  $P_{ee}$  which is independent of the  $^{239}\text{Pu}$  fraction  $F_{239}$ .

In this case, we analyze the data with the least-squares statistic

$$\chi^2 = \sum_{a,b} \left( P_{ee} \sigma_{f,a}^{\text{th}} - \sigma_{f,a}^{\text{exp}} \right) (V_{\text{exp}}^{-1})_{ab} \left( P_{ee} \sigma_{f,b}^{\text{th}} - \sigma_{f,b}^{\text{exp}} \right) + \sum_{i,j} (r_i - 1) (V_{\text{SH}}^{-1})_{ij} (r_j - 1). \quad (5)$$

In the analysis of the Daya Bay evolution data there is only one parameter determined by the fit:  $P_{ee}$ . The parameters  $r_{235}$ ,  $r_{238}$ ,  $r_{239}$ , and  $r_{241}$  are nuisance parameters. In the analysis of the other reactor antineutrino data we take into account that  $P_{ee}$  depends on the neutrino mixing parameters  $\Delta m_{41}^2$  and  $\sin^2 2\vartheta_{ee}$  in the simplest 3+1 active-sterile neutrino mixing model (see Ref. [6]). Hence, in this case there are two parameters determined by the fit:  $\Delta m_{41}^2$  and  $\sin^2 2\vartheta_{ee}$ .

**235+OSC:** A variation of the cross section per fission of the antineutrino flux from  $^{235}\text{U}$  and active-sterile neutrino oscillations with a survival probability  $P_{ee}$  as in the **OSC** model.

In this case, we analyze the data with the least-squares statistic

$$\chi^2 = \sum_{a,b} \left( P_{ee} \sigma_{f,a}^{\text{th}} - \sigma_{f,a}^{\text{exp}} \right) (V_{\text{exp}}^{-1})_{ab} \left( P_{ee} \sigma_{f,b}^{\text{th}} - \sigma_{f,b}^{\text{exp}} \right) + \sum_{i,j=238,239,241} (r_i - 1) (V_{\text{SH}}^{-1})_{ij} (r_j - 1). \quad (6)$$

In the analysis of the Daya Bay evolution data there are two parameters determined by the fit:  $r_{235}$  and  $P_{ee}$ . The parameters  $r_{238}$  and  $r_{241}$  are nuisance parameters. In the analysis of the other reactor antineutrino data we take into account that  $P_{ee}$  depends on  $\Delta m_{41}^2$  and  $\sin^2 2\vartheta_{ee}$  as in the **OSC** model. Therefore, in this case there are three parameters determined by the fit:  $r_{235}$ ,  $\Delta m_{41}^2$ , and  $\sin^2 2\vartheta_{ee}$ .

**239+OSC:** This model is similar to the **235+OSC** model, with  $^{235}\text{U} \leftrightarrow ^{239}\text{Pu}$ . The number of parameters determined by the fit is two in the analysis of the Daya Bay evolution data ( $r_{239}$  and  $P_{ee}$ ) and three in the analysis of the other reactor antineutrino data ( $r_{239}$ ,  $\Delta m_{41}^2$ , and  $\sin^2 2\vartheta_{ee}$ ).

In Section II we analyze the Daya Bay evolution data, in Section III we analyze the reactor antineutrino data which were available before the release of the Daya Bay fuel evolution data in Ref. [1], and in Section IV we perform the combined analysis.

## II. DAYA BAY EVOLUTION

The results of the different fits of the Daya Bay evolution data are given in Tab. I where we list the values

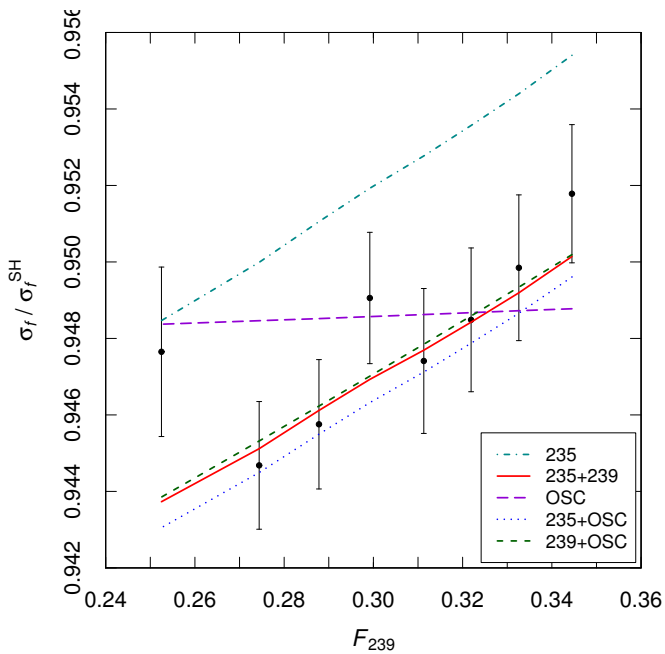


FIG. 1. Fits of the Daya Bay evolution data [1] normalized to the Saclay-Huber theoretical predictions [2–4]. The error bars show only the uncorrelated statistical uncertainties.

of the minimum  $\chi^2$ , the number of degrees of freedom and the goodness-of-fit. In Tab. I we also list the best-fit values of the fitted parameters.

Figure 1 shows the comparison of the different fits with the Daya Bay evolution data normalized to the Saclay-Huber theoretical cross sections per fission [2–4]. Note that the Daya Bay evolution data have the following two important features:

- F1:** A suppression of  $\sigma_f$  with respect to  $\sigma_f^{\text{SH}}$  in agreement with the reactor antineutrino anomaly. This feature can be fitted with at least one of the  $r_i$  and  $P_{ee}$  smaller than one (if the others are equal to one).
- F2:** An increase of  $\sigma_f / \sigma_f^{\text{SH}}$  with  $F_{239}$ . This feature can be fitted if

$$\frac{d}{dF_{239}} \frac{\sigma_{f,a}^{\text{th}}}{\sigma_{f,a}^{\text{SH}}} > 0, \quad (7)$$

where

$$\sigma_{f,a}^{\text{SH}} = \sum_i F_i^a \sigma_{f,i}^{\text{SH}}. \quad (8)$$

	<b>235</b>	<b>235+239</b>	<b>OSC</b>	<b>235+OSC</b>	<b>239+OSC</b>
$\chi_{\min}^2$	3.8	3.6	9.5	3.6	3.8
NDF	7	6	7	6	6
GoF	80%	73%	22%	72%	71%
$P_{ee}$	–	–	0.942	0.984	0.928
$r_{235}$	0.927	0.922	–	0.937	–
$r_{239}$	–	0.974	–	–	1.094

TABLE I. Fits of the Daya Bay evolution data [1].

The inequality (7) is satisfied for

$$\sum_i \frac{dF_i^a}{dF_{239}} r_i \sigma_{f,i}^{\text{SH}} > \frac{\sigma_{f,a}^{\text{th}}}{\sigma_{f,a}^{\text{SH}}} \frac{d\sigma_{f,a}^{\text{SH}}}{dF_{239}}, \quad (9)$$

with

$$\frac{d\sigma_{f,a}^{\text{SH}}}{dF_{239}} \simeq -2.4 < 0. \quad (10)$$

From Tab. I one can see that all the fits have acceptable goodness-of-fit, but the **OSC** fit corresponding to active-sterile oscillations has a goodness-of-fit which is significantly lower than the others, because it corresponds to a constant  $\sigma_f / \sigma_f^{\text{SH}}$  and cannot fit feature **F2**.

The results of our analysis agree with the conclusion of the Daya Bay collaboration [1] that the **235** model fits well the data and little is gained by allowing also the variation of  $\sigma_{f,239}$  in the **235+239** model. The shift in Fig. 1 of the line corresponding to the **235** model with respect to an ideal line fitting the data by eye is allowed by the large correlated systematic uncertainties of the Daya Bay bins [1].

The excellent fit in the **235** model is due to the fact that it can fit the two features of the Daya Bay evolution data listed above. It can obviously fit feature **F1** with  $r_{235} < 1$ . It can also fit feature **F2**, because for  $r_{235} < 1$  and  $r_{238} = r_{239} = r_{241} = 1$  the condition (9) becomes

$$-\frac{dF_{235}^a}{dF_{239}} > -\frac{d\sigma_{f,a}^{\text{SH}}}{dF_{239}} \frac{F_{235}^a}{\sigma_{f,a}^{\text{SH}}}. \quad (11)$$

This condition is satisfied, because numerically the left-hand side is about 1.30 and the right-hand side is between 0.20 and 0.24.

Obviously, the **235+OSC** model can provide a fit which is at least as good as the **235** model, with the additional possibility to improve the fit of feature **F1** with  $P_{ee} < 1$ .

It is maybe more surprising that also the **239+OSC** model fits better than the **235** model for  $r_{239} > 1$ . This can happen because the condition (9) for fitting feature **F2** is always satisfied for  $r_{239} > 1$  and  $r_{235} = r_{238} = r_{241} = 1$ . Then, a sufficiently small value of  $P_{ee} < 1$  allows us to fit feature **F1** in spite of the increase of  $\sigma_{f,a}^{\text{th}}$  due to  $r_{239} > 1$ .

Nested models can be compared in the frequentist approach by calculating the  $p$ -value of the  $\chi_{\min}^2$  difference, which has a  $\chi^2$  distribution corresponding to the difference of the number of degrees of freedom of the two models. With this method we can compare only the nested models **235** and **235+OSC**, because the  $\chi^2$  in Eq. (3) can be obtained from that in Eq. (6) with the constraint  $P_{ee} = 1$ . In this comparison, we have  $\Delta\chi^2 = 0.2$  with one degree of freedom. Hence, the null hypothesis **235** cannot be rejected in favor of the alternative more complex hypothesis **235+OSC**.

Also non-nested models can be compared considering the  $\chi_{\min}^2$  difference, but one must calculate the  $p$ -value

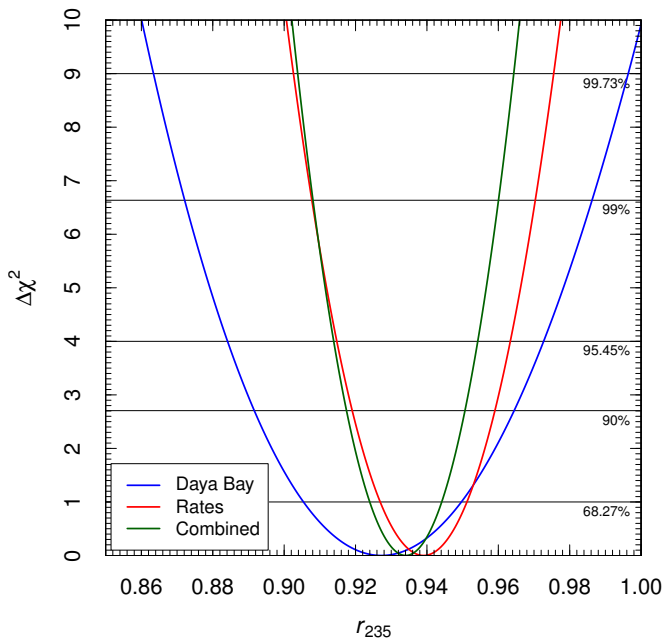


FIG. 2. Marginal  $\Delta\chi^2 = \chi^2 - \chi_{\min}^2$  for the factor  $r_{235}$  obtained from the fit of the Daya Bay evolution data [1] (Daya Bay), from the fit of the reactor rates (Rates), and from the combined fit (Combined) with the **235** model.

with a Monte Carlo. In this case one must consider as the null hypothesis the model which has the higher  $\chi_{\min}^2$  and generate many sets of synthetic data assuming the null hypothesis. The fits of all the sets of synthetic data with the two models under consideration gives the distribution of the  $\chi_{\min}^2$  difference from which one can calculate the  $p$ -value of the observed  $\chi_{\min}^2$  difference.

We do not bother to consider the comparison of the **235** and **235+239** models, since the small  $\Delta\chi_{\min}^2 = 0.2$  cannot lead to the rejection of the null hypothesis **235**.

On the other hand, it is interesting to compare the **OSC** and **235** models which have  $\Delta\chi_{\min}^2 = 5.7$ . According to our Monte Carlo simulation, the  $p$ -value of the null hypothesis **OSC** is 0.85%. Hence, the comparison of the **OSC** and **235** models disfavors the **OSC** model at the  $2.6\sigma$  level.

We also compared with a Monte Carlo the **OSC** and **235+239** models which have  $\Delta\chi_{\min}^2 = 5.9$ . We found that the null hypothesis **OSC** has a  $p$ -value of 1.3%, which is larger than in the previous case because the **235+239** model has one parameter more than the **235** model. Thus, in this case, the **OSC** model is disfavored at the  $2.5\sigma$  level, which is slightly less stringent than the  $2.8\sigma$  obtained by the Daya Bay collaboration [1] without considering the theoretical uncertainties.

Figures 2, 3, 4, 5, and 6 show the allowed regions of the fitted parameters in the **235**, **235+239**, **OSC**, **235+OSC**, and **239+OSC** models, respectively. In these figures, the results of the fit of the Daya Bay evolution data are compared with those of the fit of the reactor rates discussed in Section III and those of the combined

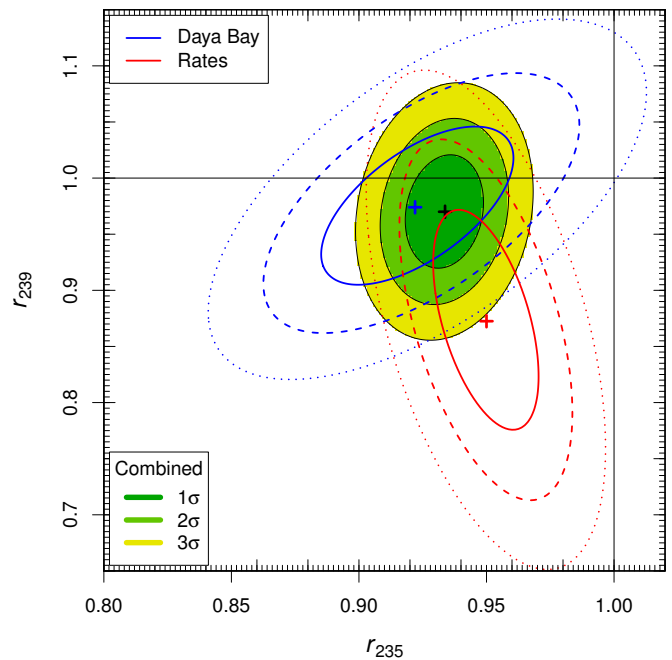


FIG. 3. Allowed regions in the  $r_{235}$ - $r_{239}$  plane obtained from the fit of the Daya Bay evolution data [1] (Daya Bay), from the fit of the reactor rates (Rates), and from the combined fit (Combined) with the **235+239** model. The best fit points are indicated by crosses. For the Daya Bay and Rates fits the  $1\sigma$ ,  $2\sigma$ , and  $3\sigma$  allowed regions are limited, respectively, by solid, dashed, and dotted lines.

fit discussed in Section IV.

From Fig. 2, one can see that assuming the **235** model, the fit of the Daya Bay evolution data gives

$$r_{235} = 0.927 \pm 0.022, \quad (12)$$

which determines the  $^{235}\text{U}$  cross section per fission to be

$$\sigma_{f,235} = 6.20 \pm 0.15. \quad (13)$$

In the case of the **235+239** model, Fig. 3 show that the Daya Bay evolution data indicate a larger suppression of  $\sigma_{f,235}$  than  $\sigma_{f,239}$ , in agreement with the results of the analysis of the Daya Bay collaboration [1]. We obtained

$$r_{235} = 0.922 \pm 0.025, \quad (14)$$

$$r_{239} = 0.974 \pm 0.046, \quad (15)$$

which imply

$$\sigma_{f,235} = 6.17 \pm 0.16, \quad (16)$$

$$\sigma_{f,239} = 4.29 \pm 0.20. \quad (17)$$

These results are compatible with those obtained by the Daya Bay collaboration [1], taking into account of the different assumptions on the uncertainties of  $\sigma_{f,238}$  and  $\sigma_{f,241}$  (10% in the calculation of the Daya Bay collaboration and the Saclay+Huber theoretical values [2–4] 8.15% and 2.60% in our calculation).

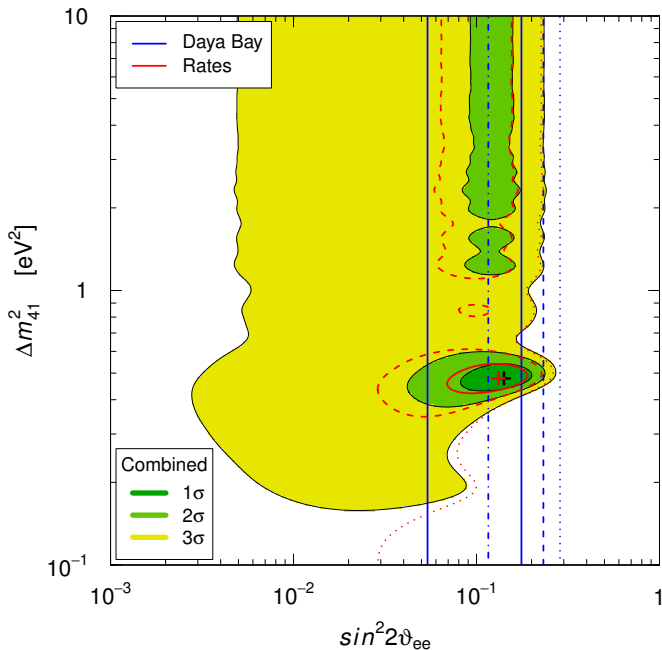


FIG. 4. Allowed regions in the  $\sin^2 2\vartheta_{ee} - \Delta m_{41}^2$  plane obtained from the fit of the Daya Bay evolution data [1] (Daya Bay), from the fit of the reactor rates (Rates), and from the combined fit (Combined) with the **OSC** model. The best fit points are indicated by crosses, except for the fit of the Daya Bay evolution data for which the best fit is the vertical dash-dotted line. For the Daya Bay and Rates fits the  $1\sigma$ ,  $2\sigma$ , and  $3\sigma$  allowed regions are limited, respectively, by solid, dashed, and dotted lines.

The vertical lines in Fig. 4 show the bounds on  $\sin^2 2\vartheta_{ee} = 2(1 - P_{ee})$  obtained in the **OSC** analysis of the Daya Bay evolution data, in which oscillations are averaged because of the large source-detector distance. One can see that

$$\sin^2 2\vartheta_{ee} = 0.12 \pm 0.06, \quad (18)$$

and there is no lower bound at  $2\sigma$ , because oscillations are favored over the no-oscillation case only at the  $1.9\sigma$  level.

Figure 5 shows that the variation of  $r_{235}$  in the **235+OSC** model causes a shift of the allowed region for  $\sin^2 2\vartheta_{ee}$  towards lower values with respect to Fig. 4 obtained with the **OSC**. In Fig. 5 there is no lower bound at  $1\sigma$ , because oscillations are favored over the no-oscillation case only at  $0.4\sigma$ . This is due to the preference for values of  $r_{235}$  smaller than one, as shown by the best-fit value in Tab. I.

On the other hand, in Fig. 6 corresponding to the **239+OSC** there is a shift of the allowed region for  $\sin^2 2\vartheta_{ee}$  towards larger values with respect to Fig. 4 obtained with the **OSC**, because  $P_{ee}$  is smaller in order to compensate the increase of  $\sigma_{f,a}^{\text{th}}$  due to  $r_{239} > 1$ .

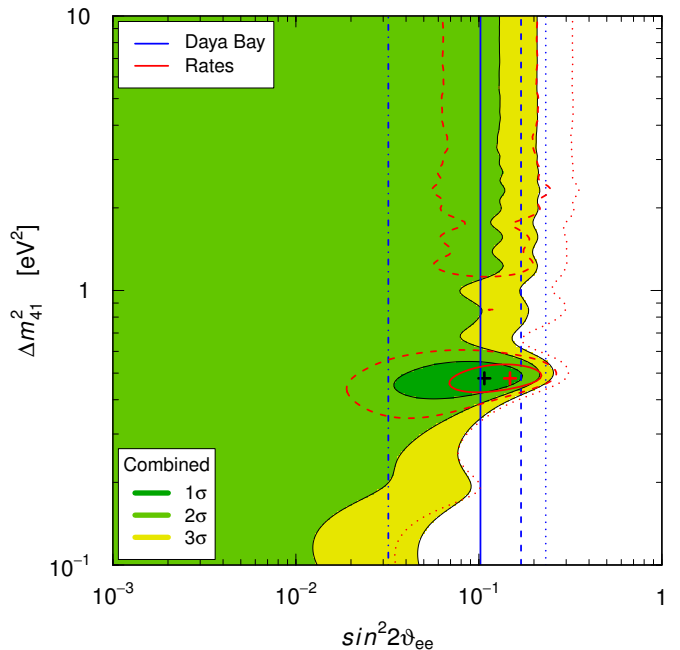


FIG. 5. Allowed regions in the  $\sin^2 2\vartheta_{ee} - \Delta m_{41}^2$  plane obtained from the fit of the Daya Bay evolution data [1] (Daya Bay), from the fit of the reactor rates (Rates), and from the combined fit (Combined) with the **235+OSC** model. The best fit points are indicated by crosses, except for the fit of the Daya Bay evolution data for which the best fit is the vertical dash-dotted line. For the Daya Bay and Rates fits the  $1\sigma$ ,  $2\sigma$ , and  $3\sigma$  allowed regions are limited, respectively, by solid, dashed, and dotted lines.

### III. PREVIOUS REACTOR RATES

In this section we consider the reactor antineutrino data which were available before the release of the Daya Bay fuel evolution data in Ref. [1]. We use the data listed in Table 1 of Ref. [5] of the following experiments: Bugey-4 [7], Rovno91 [8], Bugey-3 [9], Gosgen [10], ILL [11, 12], Krasnoyarsk87 [13], Krasnoyarsk94 [14, 15], Rovno88 [16], SRP [17], Nucifer [18], Chooz [19], Palo Verde [20], Daya Bay [21], RENO [22], and Double Chooz [23]. The Daya Bay data in Ref. [21] are relative to the average Daya Bay fuel fractions for the corresponding detection time.

The results of the fits with the models described in Section I are listed in Tab. II and the fit of the data is

	<b>235</b>	<b>235+239</b>	<b>OSC</b>	<b>235+OSC</b>	<b>239+OSC</b>
$\chi_{\min}^2$	20.7	17.7	12.8	12.6	12.7
NDF	25	24	24	23	23
GoF	71%	82%	100%	100%	100%
$\Delta m_{41}^2$	—	—	0.48	0.48	0.48
$\sin^2 2\vartheta_{ee}$	—	—	0.13	0.15	0.14
$r_{235}$	0.939	0.950	—	1.025	—
$r_{239}$	—	0.873	—	—	1.036

TABLE II. Fits of the reactor rates in Table 1 of Ref. [5].

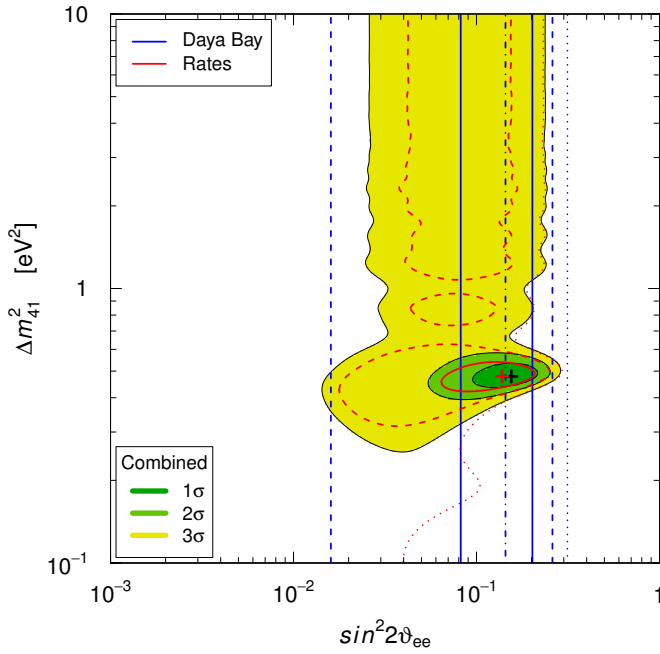


FIG. 6. Allowed regions in the  $\sin^2 2\theta_{ee} - \Delta m_{41}^2$  plane obtained from the fit of the Daya Bay evolution data [1] (Daya Bay), from the fit of the reactor rates (Rates), and from the combined fit (Combined) with the **239+OSC** model. The best fit points are indicated by crosses, except for the fit of the Daya Bay evolution data for which the best fit is the vertical dash-dotted line. For the Daya Bay and Rates fits the  $1\sigma$ ,  $2\sigma$ , and  $3\sigma$  allowed regions are limited, respectively, by solid, dashed, and dotted lines.

illustrated in Figs. 7 and 8.

From Tab. II one can see that all the model have an excellent goodness-of-fit, but the models **OSC**, **235+OSC**, and **239+OSC** with active-sterile neutrino oscillations have a significantly lower value of  $\chi_{\min}^2$ . This is due to the different source-detector distances in the experiments. As one can see from Fig. 7, where the reactor data are ordered by increasing values of the source-detector distance  $L$ . One can see that active-sterile oscillations can fit better the data of the short-baseline experiments which have a source detector distance between about 10 and 100 m. On the other hand, the poor fit of the data with the **235** model is explained by the lack of a trend Fig. 8, where the reactor data are ordered by decreasing values of  $F_{235}$ .

The comparison of the nested models **235** and **235+OSC** give  $\Delta\chi_{\min}^2 = 8.1$  with two degrees of freedom. Hence, the  $p$ -value of the null hypothesis **235** is 1.7% and it can be rejected in favor of the introduction of active-sterile neutrino oscillations at  $2.4\sigma$ . As a check, with a Monte Carlo simulation we obtained a  $p$ -value of 1.3%, which corresponds to  $2.5\sigma$ .

The **235** and **OSC** models have  $\Delta\chi_{\min}^2 = 7.9$  and our Monte Carlo comparison disfavors the null hypothesis **235** at  $3.1\sigma$ .

The **235+239** and **OSC** models have  $\Delta\chi_{\min}^2 = 4.9$

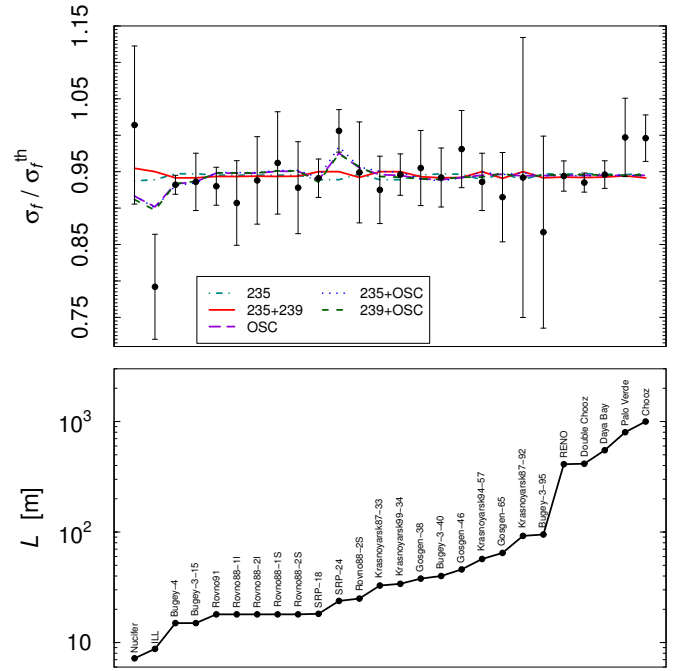


FIG. 7. The top panels show the fits of the reactor rates in Table 1 of Ref. [5]. The data are ordered by increasing values of the source-detector distance  $L$ , shown in the bottom panel. The error bars show to the experimental uncertainties.

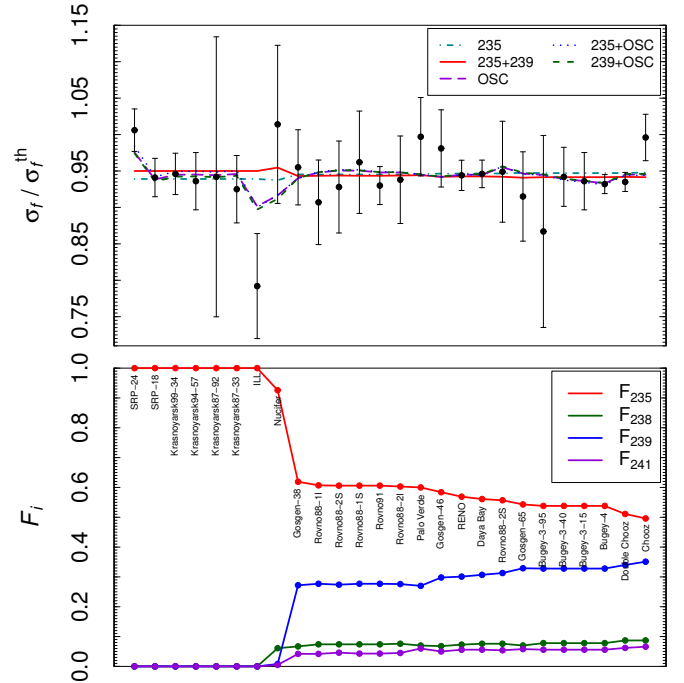


FIG. 8. The top panels show the fits of the reactor rates in Table 1 of Ref. [5]. The data are ordered by decreasing values of  $F_{235}$ , shown in the bottom panel. The error bars show to the experimental uncertainties.

and our Monte Carlo comparison disfavors the null hypothesis **235+239** at  $2.8\sigma$ .

Figure 2 shows the marginal  $\Delta\chi^2 = \chi^2 - \chi_{\min}^2$  for the factor  $r_{235}$  obtained from the fit of the reactor rates in the **235** model. The result is

$$r_{235} = 0.939 \pm 0.012, \quad (19)$$

which gives

$$\sigma_{f,235} = 6.28 \pm 0.08. \quad (20)$$

This is a determination of  $\sigma_{f,235}$  with smaller uncertainty than that obtained in Eq. (13) from the Daya Bay evolution data.

Figure 3 shows that in the case of the **235+239** model the determination of  $r_{235}$  and  $r_{239}$  is quite different in the analyses of the Daya Bay evolution data and the reactor rates. In the first analysis  $r_{235}$  and  $r_{239}$  are correlated, whereas in the second analysis they are slightly anticorrelated. Moreover, the analysis of the reactor rates prefers a larger value of  $r_{235}$  and a smaller value of  $r_{239}$  than the analysis of the Daya Bay evolution data. The results of the analysis of the reactor rates are

$$r_{235} = 0.950 \pm 0.013, \quad (21)$$

$$r_{239} = 0.873 \pm 0.064, \quad (22)$$

which imply

$$\sigma_{f,235} = 6.36 \pm 0.09, \quad (23)$$

$$\sigma_{f,239} = 3.84 \pm 0.28. \quad (24)$$

Figure 4 show the allowed region in the  $\sin^2 2\vartheta_{ee} - \Delta m_{41}^2$  plane obtained from the fit of the reactor rates in the **OSC** model. One can see that there is only one region allowed at  $1\sigma$  around the best-fit point given in Tab. II, but the  $2\sigma$  allowed regions do not have an upper bound for  $\Delta m_{41}^2$ . The  $3\sigma$  allowed region does not have a lower bound for  $\sin^2 2\vartheta_{ee}$ , because oscillations are favored over the no-oscillation case only at the  $2.7\sigma$  level.

From a comparison of Figs. 4, 5, and 6 one can see that the variations of  $r_{235}$  and  $r_{239}$  in the **235+OSC** and **239+OSC** models, respectively, have small effects on the allowed region in the  $\sin^2 2\vartheta_{ee} - \Delta m_{41}^2$  plane, in agreement with the best-fit values close to one of  $r_{235}$  and  $r_{239}$  in Tab. II.

#### IV. COMBINED ANALYSIS

In this section we present the results of the combined fits of the reactor rates in Table 1 of Ref. [5] (without the 2016 Daya Bay rate) and the 2017 Daya Bay evolution data [1].

The results of the fits with the models described in Section I are listed in Tab. III.

From Tab. III one can see that all the models have an excellent goodness-of-fit. The **OSC** model has a better goodness-of-fit than the **235** model. There is little improvement of the goodness-of-fit from the **235** model

to the **235+239** model, whereas the goodness-of-fit improves significantly in the **235+OSC** model and especially in the **239+OSC** model.

The comparison of the nested models **235** and **235+OSC** give  $\Delta\chi^2 = 5.1$  with two degrees of freedom. Hence, the  $p$ -value of the null hypothesis **235** is 7.8% and it can be rejected in favor of the introduction of active-sterile neutrino oscillations only at  $1.8\sigma$ . As a check, with a Monte Carlo simulation we obtained a  $p$ -value of 5.1%, which corresponds to  $1.9\sigma$ .

The **235** and **235+239** models have  $\Delta\chi_{\min}^2 = 2.3$  and 1.8 with respect to the **OSC** model and our Monte Carlo comparison disfavors them at  $1.7\sigma$  and  $2.2\sigma$ , respectively.

The **235**, **235+239**, **OSC**, and **235+OSC** models have  $\Delta\chi_{\min}^2 = 7.8$ , 7.3, 5.5, and 2.7 with respect to the **239+OSC** model and our Monte Carlo comparison disfavors them at  $4.2\sigma$ ,  $2.9\sigma$ ,  $2.4\sigma$ , and  $3.5\sigma$ , respectively.

From Fig. 2 one can see that in the **235** model the combined fit indicates a value of  $r_{235}$  intermediate between those obtained from the analyzes of the Daya Bay evolution data and the reactor rates. The result is

$$r_{235} = 0.934 \pm 0.010, \quad (25)$$

which gives

$$\sigma_{f,235} = 6.25 \pm 0.07. \quad (26)$$

This is a determination of  $\sigma_{f,235}$  with smaller uncertainty than that obtained in Eq. (13) from the Daya Bay evolution data and that obtained in Eq. (20) from the reactor rates.

Figure 3 shows that in the case of the **235+239** model the determination of  $r_{235}$  and  $r_{239}$  from the combined fit improves the uncertainties of the two parameters with respect to those obtained from the separate analyses of the Daya Bay evolution data and the reactor rates. The results are

$$r_{235} = 0.934 \pm 0.009, \quad (27)$$

$$r_{239} = 0.970 \pm 0.032, \quad (28)$$

which give

$$\sigma_{f,235} = 6.25 \pm 0.06, \quad (29)$$

$$\sigma_{f,239} = 4.27 \pm 0.14. \quad (30)$$

	<b>235</b>	<b>235+239</b>	<b>OSC</b>	<b>235+OSC</b>	<b>239+OSC</b>
$\chi_{\min}^2$	25.3	24.8	23.0	20.2	17.5
NDF	32	31	31	30	30
GoF	79%	78%	85%	91%	100%
$\Delta m_{41}^2$	—	—	0.48	0.48	0.48
$\sin^2 2\vartheta_{ee}$	—	—	0.14	0.11	0.15
$r_{235}$	0.934	0.934	—	0.987	—
$r_{239}$	—	0.970	—	—	1.099

TABLE III. Fits of the reactor rates in Table 1 of Ref. [5] (without the 2016 Daya Bay rate) and the 2017 Daya Bay evolution data [1].

Within the uncertainties, these results are compatible with those obtained in Ref. [24] with different assumptions on the uncertainties of  $\sigma_{f,238}$  and  $\sigma_{f,241}$ . Note that here we performed a full analysis of the Daya Bay evolution data using the complete information available in the Supplemental Material of Ref. [1] whereas in Ref. [24] the Daya Bay evolution data have been taken into account with a Gaussian approximation of the  $\chi^2$  distribution in Fig. 3 of Ref. [1].

Figure 4 show the allowed region in the  $\sin^2 2\vartheta_{ee}-\Delta m_{41}^2$  plane in the **OSC** model. The allowed regions are smaller than those obtained from the fit of the reactor rates and there is a  $3\sigma$  lower bound for  $\sin^2 2\vartheta_{ee}$ , because oscillations are favored over the no-oscillation case at the  $3.1\sigma$  level. However, there is no upper bound for  $\Delta m_{41}^2$  at  $2\sigma$ , because at that confidence level the data can be fitted with an averaged oscillation probability which does not depend on the source-detector distance.

Comparing Figs. 4 and 5, one can see that the variation of  $r_{235}$  in the **235+OSC** enlarges the allowed regions towards lower values of  $\sin^2 2\vartheta_{ee}$  and there is no lower bound for  $\sin^2 2\vartheta_{ee}$  at  $2\sigma$ , because oscillations are favored over the no-oscillation case only at  $1.4\sigma$ . This is due to the preference for values of  $r_{235}$  smaller than one, as shown by the best-fit value in Tab. III.

Figure 6 shows that the best-fitting model **239+OSC** gives the strongest indication in favor of oscillations, which are favored over the no-oscillation case at  $3.0\sigma$ . This is due to the preference for values of  $r_{239}$  larger than one, as shown by the best-fit value in Tab. III.

## V. CONCLUSIONS

In this paper we analyzed the Daya Bay evolution data [1] in the **235**, **235+239**, **OSC**, **235+OSC**, and **239+OSC** models described in Section I, which allow to compare the fits of the data under the hypotheses of variations of the  $^{235}\text{U}$  and  $^{239}\text{Pu}$  reactor antineutrino fluxes with respect to the Saclay+Huber theoretical value [2–4] and short-baseline active-sterile neutrino oscillations, taking into account the theoretical uncertainties of the reactor antineutrino fluxes. We found that the best explanation of the Daya Bay evolution data is the **235** model with a variation of the  $^{235}\text{U}$  flux with respect to the Saclay+Huber theoretical value [2–4]. Comparing the **OSC** model of active-sterile neutrino oscillations with the **235** model, we found that it is disfavored at  $2.6\sigma$ .

We also compared the **OSC** model with the **235+239** model which allows independent variations of the  $^{235}\text{U}$  and  $^{239}\text{Pu}$  fluxes with respect to Saclay+Huber theoretical values [2–4]. We found that the **OSC** model is disfavored at  $2.5\sigma$ . This result is slightly less stringent than the  $2.8\sigma$  obtained by the Daya Bay collaboration [1] without considering the theoretical uncertainties.

The Daya Bay evolution data can also be fitted well with the **235+OSC** model, with a suppression of the  $^{235}\text{U}$  flux and neutrino oscillations, or with the

**239+OSC** model, with an enhancement of the  $^{239}\text{Pu}$  flux and relatively large neutrino oscillations.

We also performed a similar analysis of the reactor antineutrino data which were available before the release of the Daya Bay fuel evolution data in Ref. [1]. In this case, we found that the best explanation of the data is the **OSC** model with active-sterile neutrino oscillations, which depend on the source-detector distance and fit the rates measured by reactor experiments with a source-detector distance between about 10 and 100 m better than the distance-independent suppression of the reactor antineutrino flux given by suppressions of the  $^{235}\text{U}$  and  $^{239}\text{Pu}$  fluxes. In this case, the **235** model with a suppression of the  $^{235}\text{U}$  flux only is disfavored at  $3.1\sigma$  and the **235+239** model with independent suppressions of the  $^{235}\text{U}$  and  $^{239}\text{Pu}$  fluxes is disfavored at  $2.8\sigma$ . As with the fit of the Daya Bay evolution data, composite models including both variations of the  $^{235}\text{U}$  or  $^{239}\text{Pu}$  fluxes and active-sterile oscillations provide good fits to the global reactor rate data.

Finally, we performed combined fits of the Daya Bay evolution data and the other reactor rates and we found that all the considered models fit well the data. The **OSC** model has a better goodness-of-fit than the **235** and **235+239** models, which are almost equivalent. We obtained better fits of the data with the composite **235+OSC** and **239+OSC** models. In particular, the best-fit model is **239+OSC**, with an increase of the  $^{239}\text{Pu}$  flux with respect to the Saclay+Huber theoretical value [2–4] and relatively large active-sterile neutrino oscillations.

In conclusion, although the recent Daya Bay evolution data [1] disfavor short-baseline active-sterile neutrino oscillations over a suppression of the  $^{235}\text{U}$  reactor antineutrino flux or independent suppressions of the  $^{235}\text{U}$  and  $^{239}\text{Pu}$  fluxes, the result is reversed in the analysis of the other available reactor antineutrino data. Both sets of data are individually well-fitted by composite models with variations of the  $^{235}\text{U}$  or  $^{239}\text{Pu}$  fluxes and active-sterile neutrino oscillations. The combined data set indicates a preference for the composite models and, in particular, the best fit is obtained with the **239+OSC** model, through an enhancement of the  $^{239}\text{Pu}$  flux and relatively large oscillations. However, while these combined fits suggest a preference for models including sterile neutrinos, the significant uncertainties in the reactor rate measurements and the high goodness-of-fits observed for models both with and without sterile neutrinos make it clear that the search for the explanation of the reactor antineutrino anomaly [3] still remains open. We hope that it will be solved soon by the new short-baseline reactor neutrino experiments which will measure the reactor antineutrino flux from reactors with different fuel compositions: highly enriched  $^{235}\text{U}$  research reactors for PROSPECT [25], SoLid [26], and STEREO [27], and commercial reactors with mixed fuel compositions for DANSS [28] and Neutrino-4 [29].



## ACKNOWLEDGMENT

We would like to thank the Daya Bay collaboration for useful discussions and information on the Daya Bay evolution data. The work of X.P. Ji was supported by the National Natural Science Foundation of China (Grants No. 11235006 and No. 11475093) and by the CAS Cen-

ter for Excellence in Particle Physics (CCEPP). The work of Y.F. Li was supported in part by the National Natural Science Foundation of China under Grant Nos. 11305193 and 11135009, by the Strategic Priority Research Program of the Chinese Academy of Sciences under Grant No. XDA10010100, and by CCEPP. The work of B.R. Littlejohn was partially supported by the DOE Office of Science, under award No. DE-SC0008347.

- 
- [1] F. P. An *et al.* (Daya Bay), *Phys.Rev.Lett.* **118**, 251801 (2017), arXiv:1704.01082 [physics].
- [2] T. A. Mueller *et al.*, *Phys. Rev.* **C83**, 054615 (2011), arXiv:1101.2663 [hep-ex].
- [3] G. Mention *et al.*, *Phys. Rev.* **D83**, 073006 (2011), arXiv:1101.2755 [hep-ex].
- [4] P. Huber, *Phys. Rev.* **C84**, 024617 (2011), arXiv:1106.0687 [hep-ph].
- [5] S. Gariazzo, C. Giunti, M. Laveder, and Y. Li, *JHEP* **1706**, 135 (2017), arXiv:1703.00860 [hep-ph].
- [6] S. Gariazzo, C. Giunti, M. Laveder, Y. Li, and E. Zavanin, *J. Phys.* **G43**, 033001 (2016), arXiv:1507.08204 [hep-ph].
- [7] Y. Declais *et al.* (Bugey), *Phys. Lett.* **B338**, 383 (1994).
- [8] A. Kuvshinnikov, L. Mikaelyan, S. Nikolaev, M. Skorkhvatov, and A. Etenko, *JETP Lett.* **54**, 253 (1991).
- [9] B. Achkar *et al.* (Bugey), *Nucl. Phys.* **B434**, 503 (1995).
- [10] G. Zacek *et al.* (CalTech-SIN-TUM), *Phys. Rev.* **D34**, 2621 (1986).
- [11] H. Kwon *et al.*, *Phys. Rev.* **D24**, 1097 (1981).
- [12] A. Hoummada, S. Lazrak Mikou, G. Bagieu, J. Cavaignac, and D. Holm Koang, *Applied Radiation and Isotopes* **46**, 449 (1995).
- [13] G. S. Vidyakin *et al.* (Krasnoyarsk), *Sov. Phys. JETP* **66**, 243 (1987).
- [14] G. S. Vidyakin *et al.* (Krasnoyarsk), *Sov. Phys. JETP* **71**, 424 (1990).
- [15] G. S. Vidyakin *et al.* (Krasnoyarsk), *JETP Lett.* **59**, 390 (1994).
- [16] A. I. Afonin *et al.*, *Sov. Phys. JETP* **67**, 213 (1988).
- [17] Z. D. Greenwood *et al.*, *Phys. Rev.* **D53**, 6054 (1996).
- [18] G. Boireau *et al.* (NUCIFER), *Phys. Rev.* **D93**, 112006 (2016), arXiv:1509.05610 [physics].
- [19] M. Apollonio *et al.* (CHOOZ), *Eur. Phys. J.* **C27**, 331 (2003), hep-ex/0301017.
- [20] F. Boehm *et al.* (Palo Verde), *Phys. Rev.* **D64**, 112001 (2001), hep-ex/0107009.
- [21] F. An *et al.* (Daya Bay), *Chin.Phys.* **C41**, 013002 (2017), arXiv:1607.05378 [hep-ex].
- [22] H. Seo, (2016), talk presented at AAP 2016, Applied Antineutrino Physics, 1-2 December 2016, Liverpool, UK.
- [23] Double Chooz Collaboration, Private Communication.
- [24] C. Giunti, arXiv:1704.02276 [hep-ph].
- [25] J. Ashenfelter *et al.* (PROSPECT), *J. Phys.* **G43**, 113001 (2016), arXiv:1512.02202 [physics].
- [26] N. Ryder (SoLid), *PoS EPS-HEP2015*, 071 (2015), arXiv:1510.07835 [hep-ex].
- [27] V. Helaine (STEREO), arXiv:1604.08877 [physics.ins-det].
- [28] I. Alekseev *et al.* (DANSS), *JINST* **11**, P11011 (2016), arXiv:1606.02896 [physics].
- [29] A. P. Serebrov *et al.* (Neutrino-4), *PoS INPC2016*, 255 (2017), arXiv:1702.00941 [physics.ins-det].